# Variable Kinetic Isotope Effect Reveals Multi-step Pathway for Protonolysis of a Pt–Me Bond

Irving D. Rettig, Jingtong Xu, Elizabeth A. Knight, Phan T. Truong, Miriam A. Bowring*

Department of Chemistry, Reed College, Portland, Oregon 97202, USA.

ABSTRACT: The reaction of $(cod)PtMe_2$ (cod = 1,5-cyclooctadiene) with trifluoroacetic acid (TFAH) to release methane is an important system because it represents the microscopic reverse of desirable methane activation, and because it has an unusually large kinetic isotope effect (KIE) that has been tentatively attributed to proton tunneling. A detailed kinetic and mechanistic investigation of this system was conducted using stopped-flow and traditional time-dependent UV-vis spectroscopy, supported by NMR and DFT studies. Consistently large KIE values (~14) in line with previous reports were obtained over a large range of reactant concentrations (0.1 – 1.6 mM $(cod)PtMe_2$ and 3.2 mM to 6.0 M acid). At lower concentrations of acid, the KIE decreased significantly (KIE = ~6 for 0.1 mM $(cod)PtMe_2$ and 0.2 mM acid). This concentration-dependent KIE suggests a multi-step reaction mechanism, eliminating the need to invoke proton tunneling. The reaction exhibits first-order dependence on $(cod)PtMe_2$ and approximately second-order dependence on acid, with at least 2 equivalents of acid required for complete conversion. Overall, the kinetic data indicate a multi-molecular, multi-step reaction mechanism for the protonolysis of $(cod)PtMe_2$, thus ruling out the previously accepted bimolecular single-step mechanism. A mechanistic alternative consistent with the kinetic data is proposed, in which sequential oxidative addition and reductive elimination occur, and the second equivalent of acid serves to stabilize trifluoroacetate anion in solution.
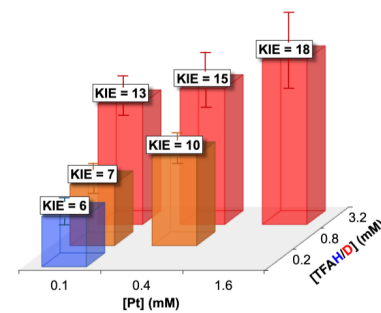
INTRODUCTION

C–H activation of methane is famously challenging, and it is necessary for the catalytic generation of liquid fuel or other value-added products from methane.[1–6] Platinum complexes have shown particular promise for mediating methane activation and functionalization.[6–15] In order to achieve improved methane activation at a platinum center, it is important to understand the possible reaction mechanisms. One key approach is to study the microscopic reverse reaction: protonolysis of a Pt–Me bond to generate methane.[16–24]

Two plausible mechanisms for the protonolysis of a Pt–Me bond in a square planar Pt(II) methyl complex have been proposed (Scheme 1), and distinguishing between the two mechanisms has proved challenging.[17–27]

Scheme 1. Proposed[20] mechanisms for methyl protonolysis by a general Pt(II) square planar complex
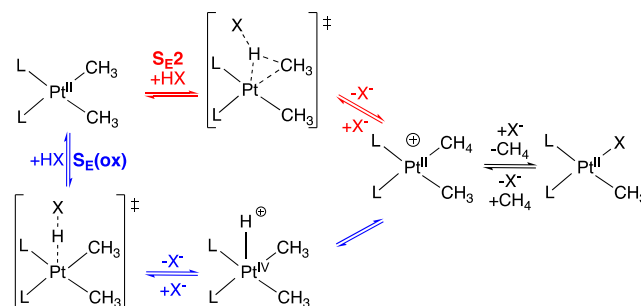
One proposed mechanism for protonolysis is the concerted mechanism (S_E2), in which the Pt–C σ bond undergoes direct electrophilic attack by an acidic proton to generate a three-centered transition state and form a methane σ-complex in a single step. Methane is released by associative displacement with the conjugate base.[28,29] The other proposed mechanism is the oxidative mechanism ($S_E(ox)$[30]), in which oxidative addition of the acid to generate a Pt(IV) hydride is followed by reductive elimination to form the Pt(II) methane σ-complex before associative displacement of methane. The two mechanisms are difficult to distinguish by kinetic measurements; even the observation of Pt hydride complexes does not mean that these species are intermediates on the reaction pathway.[17,20,21,23,31–35]

In the study of organometallic reaction mechanisms, kinetic isotope effects (KIEs, commonly defined as the ratio of rate constants k_H/k_D for a given reaction) are an

informative and widely used tool, but they are also difficult to interpret.[36–42] KIEs can be measured either by competition experiments in one reaction vessel, or by separate measurements of reaction rates for parallel reactions. Very large KIE values (*e.g.* above ~7 for a C–H bond breaking or above ~11 for an O–H bond breaking) are not accounted for by the typical simplified models of zero-point energy differences in just one bond vibration.[36,42–46] Such large KIE values have been explained by proton tunneling, complex vibrational effects, or compound effects from multiple reaction steps, but their mechanistic origins are difficult to assign.[36] In the case of protonolysis of Pt(II) complexes, researchers have observed large KIEs for many years, but have not reached a conclusive mechanistic interpretation or used them to distinguish definitively between the S_E2 and $S_E(ox)$ mechanisms.[20]

In 1978, Romeo and colleagues observed a KIE of ~6 for the protonolysis of Pt–aryl complexes with excess H(D)Cl in MeOH(D)/H$_2$(D$_2$)O by measuring separate rate constants for parallel reactions.[47,48] They concluded at the time that this relatively large KIE supported the S_E2 pathway, since the only (and therefore rate-limiting) transition state of that mechanism is proton transfer, which would be expected to have a significant KIE. After decades of further research they expanded their interpretation to propose that the large KIE is consistent with either an S_E2 pathway or an $S_E(ox)$ pathway as long as protonation is rate-limiting.[49,50,17] Puddephatt and coworkers pointed out that reductive elimination could also carry a large KIE, and therefore the large KIE does not distinguish between mechanisms.[33]

Large KIE values that vary based on reaction conditions have also been observed. The Bercaw group found that the KIE for protonolysis of (tmeda)PtMeCl (tmeda=*N,N,N',N'*-tetramethylethylenediamine) by triflic acid in methanol changed from 9.1 at 0 ºC by a competition experiment to 2.3 at -40 ºC by parallel reactions. They ascribed the large KIE to fractionation factors and stated that it could thus not be used to distinguish between the S_E2 and $S_E(ox)$ mechanisms.[16,44] Roddick and coworkers similarly observed a very large KIE of 18 ± 2 upon treatment of (dfepe)PtMe$_2$ (dfepe = (C$_2$F$_5$)$_2$PCH$_2$CH$_2$P(C$_2$F$_5$)$_2$) with a mixture of TFAH (trifluoroacetic acid, HOOCCF$_3$) and TFAD (DOOCCF$_3$) at 0 ºC, and found a much smaller KIE of 3.6(4) for the protonolysis of (dfepe)PtMe(trifluoroacetate) at 150 ºC from rates of parallel reactions with TFAH and TFAD. Like the Bercaw group, they concluded that large KIEs could arise from partitioning effects, and therefore do not distinguish between the S_E2 and $S_E(ox)$ mechanisms.[23,44,51]

It was later proposed that the S_E2 mechanism is favored for complexes featuring electron-withdrawing ligands, while the $S_E(ox)$ mechanism is likely favored for complexes with electron-donating ligands.[52] Work by the Tilset group with diimine ligands supports the $S_E(ox)$ mechanism for Pt–Me protonolysis with evidence from trapping studies and kinetic activation parameters.[24,32] The Tilset group also observed a large KIE for a related Pt–Ph system, and noted that both tunneling and

compound effects from multiple steps could be responsible for the large KIE.[53]

The Bercaw group has reported especially large KIEs for protonolysis, such as KIE = 25.9 ± 0.3 at 0 ºC for the reaction of (cod)PtMe$_2$ (**1**, cod = 1,5-cyclooctadiene) treated with a mixture of TFAH and TFAD in C$_2$D$_4$Cl$_2$ to produce (cod)PtMe(trifluoroacetate) (**2**). The KIE for the same reaction at 25 °C was reported as 18.0 ± 0.9 in CD$_2$Cl$_2$ (Scheme 2).[18–20,54] The calculated KIE for protonolysis of **1** (without tunneling corrections) was only ~5.[19]

Scheme 2. Reaction of 1 with a mixture of TFAD and TFAH in CD$_2$Cl$_2$ to produce 2 and methane.
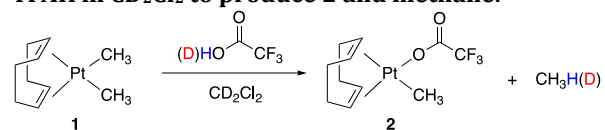
Bercaw and coworkers concluded in a combined theoretical/experimental study that the mechanism is S_E2 for this reaction. While they originally further proposed that a large KIE could be an indicator of an S_E2 mechanism more generally, they ultimately published a report titled "Large Kinetic Isotope Effects for the Protonolysis of Metal Methyl Complexes Are Not Reliable Mechanistic Indicators." The titular conclusion was based on the evidence that the observed KIE for a series of metal–methyl complexes did not correlate with their ability to undergo oxidative addition. The Bercaw group ascribed the large KIE for protonolysis of **1** to possible proton tunneling, while emphasizing that many factors can contribute to large KIE values.

Two additional density functional theory (DFT) studies of the protonolysis of **1** also support the S_E2 mechanism. Mai and Kim showed that a computational model of the S_E2 mechanism with a multidimensional tunneling correction produced similar KIE and activation parameters as observed experimentally by the Bercaw group, and they concluded that a large KIE could generally indicate an S_E2 pathway with tunneling.[55] A broader computational study of Pt–Me protonolysis also supported an S_E2 mechanism for protonolysis of **1**, while showing that $S_E(ox)$ may be at play for other systems.[56] Experimentalists have used these theoretical results in interpreting new data: Puddephatt and coworkers more recently observed a very large KIE of about 40 for the protonolysis of a Pt–alkyl bond at 25 ºC for parallel reactions in CH$_3$OH or CH$_3$OD, and based on the theoretical work from Mai and Kim connecting a large KIE to the S_E2 mechanism, they suggested an S_E2 pathway with tunneling.[21,27]

Despite the nearly half-century of progress described, both the mechanism for Pt–Me bond protonolysis and the cause of the large observed KIEs have remained uncertain. The leading proposed mechanism for protonolysis of **1** by TFAH(D) is a concerted S_E2 mechanism with proton tunneling. We report herein a detailed kinetic and mechanistic analysis of the reaction of **1** with TFAH(D). Our most surprising observations include a large apparent KIE that varies based on reactant concentrations, and approximately second-order dependence of reaction rate on acid concentration.

We conclude that the reaction mechanism involves multiple reaction steps, as does the $S_E(ox)$ mechanism, and also multiple acid molecules, a mechanistic feature that has not been previously considered. Because of the multi-step, multi-molecular mechanism, the large apparent KIE can be explained by compound isotope effects; proton tunneling need not be invoked. We hope that this mechanistic explanation for the large KIE in Pt–Me protonolysis will prove broadly useful in further experimental investigation and interpretation of large KIEs in organometallic systems and in the understanding of C–H activation mechanisms.

RESULTS AND DISCUSSION

To replicate the large KIE measurement by Bercaw and coworkers for the protonolysis of **1** by competition experiment, compound **1** was treated with a large excess of acid, in a ratio of 170:17:1 TFAD:TFAH:**1**, in CD_2Cl_2 (Scheme 2). The KIE was then calculated from the ratio of the dissolved products CH_4 and CH_3D as determined by ^{1}H NMR integration and averaged across three runs. The KIE was calculated to be 12.0 ± 0.5. We identified an arithmetic error in the original report by Bercaw et. al.; the corrected KIE value of about 13.5 for their experiments is comparable to our results.[20,54]

Next, we repeated the competition experiment in triplicate using a much smaller 17:17:1 ratio of TFAH:TFAD:**1**. The observed KIE dropped significantly to 7.9 ± 0.2. Trials at lower total acid concentrations indicated even lower KIE values. This observation that the observed KIE changes was an early indication that the reaction of **1** with TFAH may be more complex than previously understood. To investigate further, we decided to make parallel measurements of the rates of protonolysis and deuterolysis of **1**. Monitoring of the reaction by ^{1}H NMR spectroscopy revealed no observable side products or intermediates (Figure S4).

We then turned to UV-vis spectroscopy to gather high resolution rate data over a range of reagent concentrations. Compound **1** (0.4 mM) was treated with TFAH or TFAD (0.5, 1.0, 1.5, 2.0, or 8.0 equiv). A solution of acid in CH_2Cl_2 was added by gas-tight syringe to a cuvette in the spectrometer containing a continuously stirred solution of **1** in CH_2Cl_2 maintained at 296 K. Reaction progress was monitored by the decay of the absorbance at 288 nm (Figure 1).[57,58]
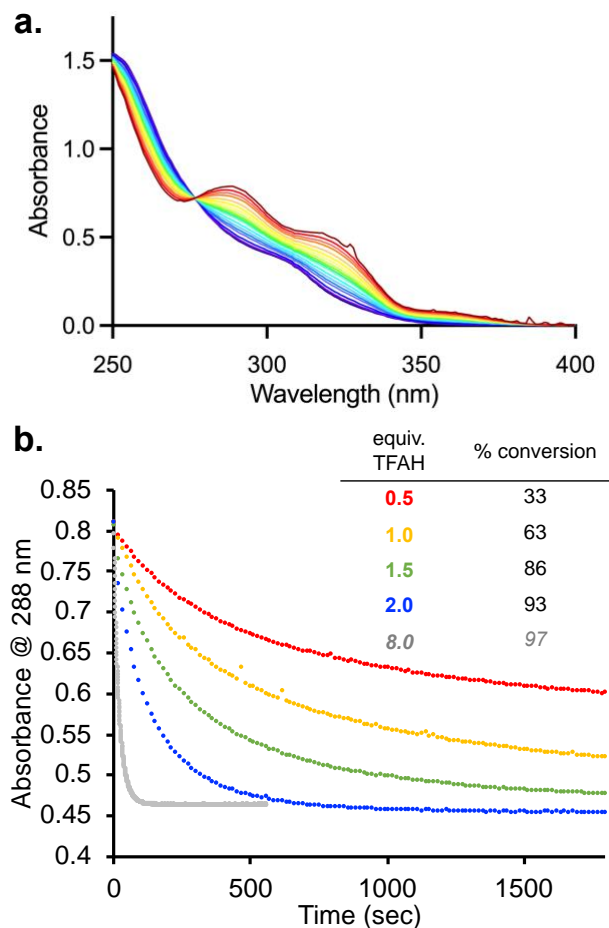

Figure 1. (a) The full absorbance profile of **1** (0.4 mM, dark red) decaying (red to purple) following treatment with TFAD (2.0 equiv). Spectra shown were collected at 3 sec intervals. (b) The plot of the decrease in the absorbance at 288 nm of a solution of **1** (0.4 mM) in CH_2Cl_2 at 296 K upon addition of 0.5, 1.0, 1.5, 2.0, and 8.0 equivalents of TFAH.

Similar decay behavior was observed for the other two λ_{max} values at 318 and 358 nm. Notably, a minimum of 2.0 equivalents of TFAH were required for the protonolysis reaction to near completion (93% conversion, compared to 63% conversion with 1 equivalent of acid). In addition, the decay profiles with 1 or 2 equivalents of acid did not fit well to a simple second-order model.[59] Preliminary KIE values determined by comparing approximate rates for reaction of **1** with 0.5 to 2 equivalents of TFAH and TFAD were lower than the values of 12-14 obtained by NMR competition experiment in which acid was used in large excess. The initial UV-vis kinetics experiments, requiring 2.0 equivalents of acid and exhibiting variable KIE, suggested that the protonolysis was not a simple bimolecular single-step reaction.

Imagining that a large excess of acid might generate simplified rate behavior, we turned to stopped-flow UV-vis spectroscopy to measure fast rates under excess acid conditions. Compound **1** (1.6 mM) was rapidly mixed with TFAH or TFAD (34, 100, 250, or 375 equiv) in the stopped-flow cell. The experiments were performed as triplicates of triplicates to confirm reproducibility.

Indeed, the absorbance decay observed under excess acid conditions fit well to a single exponential decay

(Figure 2a), providing evidence that the protonolysis reaction rate has first-order dependence on the concentration of **1**, and allowing calculation of pseudo-first-order observed rate constants.
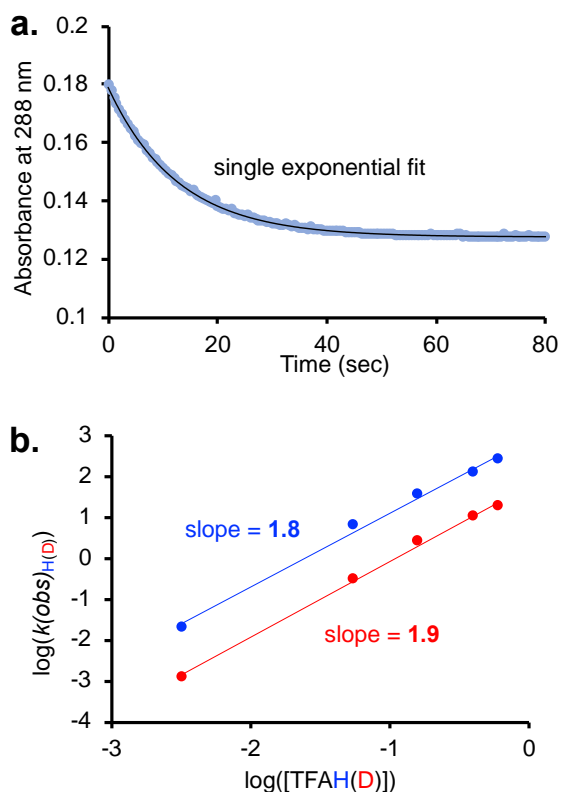

Figure 2. (a) the absorbance decay of **1** (light blue, 0.1 mM [**1**] with 32 equiv TFAH) overlaid with the nonlinear least-squares fitting of the absorbance - time profile to a first-order exponential decay (black; R^2 = 0.9998). (b) the log-log plot of $k(obs)_H$ versus [TFAH] (blue) and of $k(obs)_D$ versus [TFAD] (red) to give an order in acid of 1.8 for TFAH and 1.9 for TFAD.

KIE values were calculated from these rate constants and found to be similarly high for each of the four concentrations of acid, averaging about 14 (Table 1). The KIE remained comparable (14.3 ± 0.8) when the concentration of **1** was increased to 4.0 mM and a larger excess of acid was used (100 equivalents). The consistently large KIE values obtained from ratios of observed rate constants are similar to the reported large KIE values determined from product ratios by NMR spectroscopy (~13.5[20,54]).

The observed rate constants from stopped-flow spectroscopy under excess acid conditions were also used to calculate the order in acid from a log-log plot of the observed rate constant versus the concentration of acid. The slope of the linear regression is approximately 2 for both TFAH and TFAD, indicating approximately second-order dependence of the reaction rate on acid concentration (Figure 2b). This order is consistent with the necessity of 2 equivalents of acid for the reaction to reach completion and is further evidence that the reaction mechanism is not simply bimolecular, as had been assumed.

Table 1. Values for $k(obs)_H$, $k(obs)_D$, and KIE from stopped-flow UV-vis spectroscopy.

entry	[**1**], mM	[TFAH (D)], mM	Equiv Acid	$k(obs)_H$ (sec^{-1})	$k(obs)_D$ (sec^{-1})	KIE
1	1.6	54	34	5.1 ± 0.4	0.30 ± 0.01	16 ± 4
2	1.6	160	100	35.8 ± 0.3	2.40 ± 0.01	12.6 ± 0.7
3	1.6	400	250	134 ± 2	10.6 ± 0.1	14.9 ± 0.5
4	1.6	600	375	264 ± 4	19.5 ± 0.5	13 ± 1
5	4.0	400	100	139 ± 7	9.7 ± 0.2	14.3 ± 0.8

Once the large KIE values and the reaction order in acid and **1** had been confirmed using the high concentration conditions and stopped-flow spectroscopy, we returned to time-dependent traditional UV-vis spectroscopy to investigate the lower KIE values observed under the lower concentration conditions. The rates of protonolysis and deuterolysis of **1** were measured for a range of concentrations of **1** (0.1 to 1.6 mM) and acid (0.2 to 3.2 mM) by traditional UV-vis spectroscopy.

Absorbance decay profiles under each set of reaction conditions were measured in at least triplicate. Since the rate behavior for the protonolysis or deuterolysis of **1** without excess acid could not be modeled by simple exponential fits, observed rate constants were determined by the initial rates method when 8 or fewer equivalents of acid were used, and by a pseudo-first-order fit when 8 or more equivalents of acid were used. Both methods were used for the reactions of exactly 8 equivalents of acid, and the resulting rate constants were the same within error.

We compared initial rates from traditional UV-vis spectroscopy to the data from the stopped-flow conditions, using the same concentration of **1** (1.6 mM) and a far lower concentration of acid (3.2 mM) (Table 2, entry 1). The key final point for the log-log plot collected under the lower acid conditions falls in line with the other data and confirms that the reaction order in TFAH or TFAD is about 2 (Figure 2b), so the mechanism may involve two molecules of acid. Additionally, the KIE (18 ± 3) with 2 equivalents of acid (Table 2, entry 1) was consistent with the results for up to 375 equivalents of acid (Table 1). This consistency shows that the different sets of conditions are comparable and that a large excess of acid is not required for a large KIE.

The KIE values under the lower relative acid concentration conditions (3.2 mM) were consistent with the large KIE values at higher acid concentrations. A small increase in KIE values was observed when the concentration of **1** was increased (0.1, 0.4, and 1.6 mM; Table 2, entries 1,2,3; Figure 3), but since three values were either within error of each other or nearly so, further exploration was needed.

A dramatically lower KIE was revealed when we decreased the concentrations of both reagents while holding their ratio constant at 2:1 (Table 2, entries 1,4,6; Figure 3). The observed KIE decreases from 18 ± 3 to 9.8 ± 0.6 as the concentration of **1** decreases from 1.6 mM to

0.4 mM. At the lowest observed overall concentration of both reagents (0.1 mM **1** and 0.2 mM acid), the KIE is at its lowest (5.5 ± 0.2).

Table 2. Values for $k(obs)_H$, $k(obs)_D$, and KIE from time-resolved UV-vis spectroscopy.

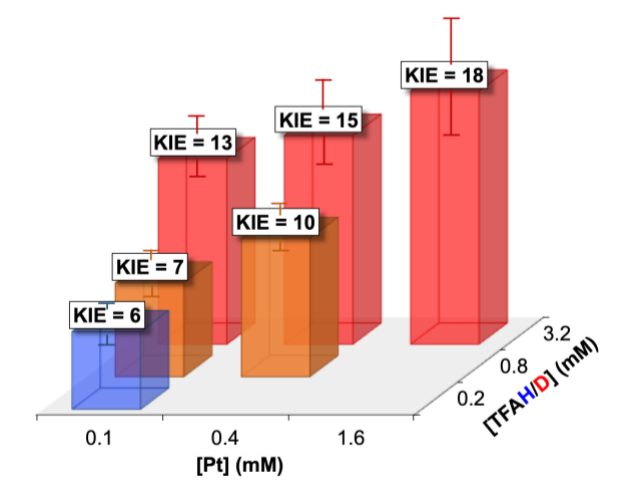| entry	[1], mM	[TFAH (D)], mM	Equiv Acid	$k(obs)_H$ $(10^{-6} sec^{-1})$	$k(obs)_D$ $(10^{-6} sec^{-1})$	KIE
1	1.6	3.2	2	140 ± 20	7.9 ± 0.6	18 ± 3
2	0.4	3.2	8	20 ± 2	1.4 ± 0.1	15 ± 1
3	0.1	3.2	32	1.8 ± 0.1	0.100 ± 0.003	13.2 ± 0.5
4	0.4	0.8	2	2.5 ± 0.1	0.30 ± 0.01	9.8 ± 0.6
5	0.1	0.8	8	0.30 ± 0.01	0.040 ± 0.001	6.7 ± 0.2
6	0.1	0.2	2	0.070 ± 0.003	0.010 ± 0.002	5.5 ± 0.9

Figure 3. Bar graph illustrating the dependence of KIE on reagent concentration.

The variable KIE was intriguing, and we sought to determine whether varying the concentration of acid alone would affect the KIE. We found that the KIE did decrease with decreasing acid concentration when the concentration of **1** was held at a low value (0.1 mM) as we moved from 32 to 8 to 2 equivalents of acid (Table 2, entries 3,5,6; Figure 3). In contrast, when the concentration of **1** was held constant at a higher value (1.6 mM), and the amount of acid was varied from excess to even larger excess (34 – 375 equivalents), the KIE values stayed about the same (Table 1). Overall, the KIE is smallest at the lowest overall concentration of both acid and **1**.

Since an elementary reaction is expected to have a constant KIE, the variable KIE observed is evidence for a multi-step reaction mechanism. Not only does a multi-step mechanism rule out the single-step S_E2 pathway, but it also provides an explanation for the large KIE values that does not rely on tunneling. The simplified classical limit for a KIE only applies to one bond and one elementary reaction step. The compound effect of KIEs and equilibrium isotope effects (EIEs) from multiple reaction steps can lead to a large overall observed KIE for a multi-step reaction.[16,23,36–41,60–67] The partitioning effects or fractionation factors mentioned by the Bercaw and Roddick groups to explain large KIEs that varied with changes in reaction conditions are only relevant under direct competition conditions, so they cannot explain the large and variable KIEs we observed as ratios of rates from parallel reactions.[16,23,44]

Once we had determined that the protonolysis reaction requires more than a single equivalent of acid (based on the reaction order and UV-vis conversion studies), we further investigated the involvement of multiple acid molecules by ^{1}H NMR spectroscopy. Compound **1** (0.02 M) was treated with TFAH (0.5, 1, or 2 equiv) in CD_2Cl_2 at room temperature (Figure 4). A singlet at 4.78 ppm with platinum satellites, corresponding to the alkene protons of complex **1**, immediately decreases and two new inequivalent singlets with platinum satellites appear 4.57 and 5.52 ppm, assigned to the alkene protons of the product (cod)PtMe(trifluoroacetate) (**2**) (Figure S1). Methane is observed as a singlet at 0.21 ppm. Even after 72 hours of additional equilibration time, only the sample with 2.0 equiv of TFAH reaches complete conversion (95%), compared to 73% with 1.0 equiv of TFAH. The ^{1}H NMR data thus further support the involvement of two acid molecules.

An additional ^{1}H NMR experiment was carried out with a large excess (100 equiv) of TFAH. The alkene resonances assigned to the cod ligand of complex **2** were shifted significantly compared to the spectrum for the sample containing only 2 equiv of acid. The excess acid was then removed under reduced pressure and an additional ^{1}H NMR spectrum collected and compared again to the sample containing 2 equiv of acid (Figure S6). The removal of excess acid resulted in a shift of both alkene signals, returning them to a chemical shift similar to that observed with 2 equiv of acid. The shift of alkene resonances for compound **2** under excess acid conditions indicates a change in electron density at the Pt center in the presence of excess TFAH, which suggests that excess TFAH in the reaction mixture interacts with the Pt complexes present.
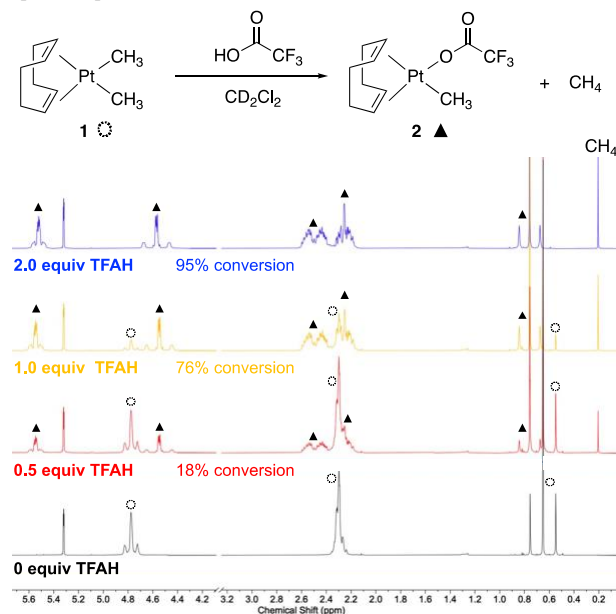
Figure 4. Stacked ^{1}H NMR spectra of the reaction mixture for the treatment of **1** (open circles) with 0.5 to 2.0 equiv of TFAH in CD$_2$Cl$_2$. The product **2** is indicated by solid triangles. The percent conversion of **1** as determined by integration relative to the internal standard 1,2,3-trimethoxybenzene for each experiment is given for each spectrum.

Taking all our experimental evidence together, we conclude that the protonolysis of **1** with TFAH proceeds by a multi-step reaction mechanism that involves more than one acid molecule, rather than the single-step bimolecular mechanism previously proposed. To imagine a possible proposed mechanism consistent with these conclusions, we considered the wealth of experimental and theoretical data on the system[18–20,55,56] alongside our own experimental data.

The established multi-step mechanistic possibility for this reaction is the S$_E$(ox) pathway. The S$_E$(ox) pathway was ruled out based on calculated energies in three separate reports, by Bercaw and coworkers, Mai and Kim, and Sicilia and coworkers, and it also only involves one acid molecule.[19,55,56] We propose that the second acid molecule could serve to make a modified S$_E$(ox) pathway possible by stabilizing the trifluoroacetate anion in solution and thus facilitating formation of a 5-coordinate Pt(IV) hydride intermediate (Scheme 3).

In calculations by Sicilia et al. and by Mai and Kim, the S$_E$(ox) pathway for the reaction of **1** with TFAH was modeled as direct formation of a 6-coordinate cationic Pt(IV) hydride intermediate (cod)PtMe$_2$(TFA)(H) (**A**), followed by direct reductive elimination from **A** to generate the cationic methane σ-complex (cod)PtMe(CH$_4$)$^+$ (**C**). In calculations by Bercaw and coworkers, the S$_E$(ox) pathway was modeled as formation of a 5-coordinate cationic Pt(IV) hydride intermediate (cod)PtMe$_2$(H)$^+$ (**B**), followed by reductive elimination to generate the same σ-complex (**C**). Each pathway was calculated to be energetically unfavorable compared to the S$_E$2 mechanism.

We propose that the 6-coordinate and 5-coordinate Pt(IV) hydride intermediates **A** and **B** could both be necessary, along with additional acid, to make the mechanism possible. The 5-coordinate intermediate **B** is necessary as a precursor to kinetically accessible reductive elimination.[19,35,68–75] At the same time, the 6-coordinate intermediate **A** is thermodynamically favored over **B** and a free trifluoroacetate anion, and would dominate an equilibrium between the two. DFT calculations show that **A** is favored relative to **B** and a free trifluoroacetate anion by over 20 kcal/mol in the absence of additional acid, but the difference is only about 11 kcal/mol when one explicit additional molecule of acid is present to interact with the trifluoroacetate anion in the product (see SI). We propose that the role of additional acid is to favor the formation of the 5-coordinate intermediate by stabilizing the TFA$^-$ anion in solution, and possibly assisting its dissociation (Scheme 3).[75–85]

Scheme 3. Modified S$_E$(ox) mechanism for reaction of 1 with TFAH, including potential role for additional TFAH
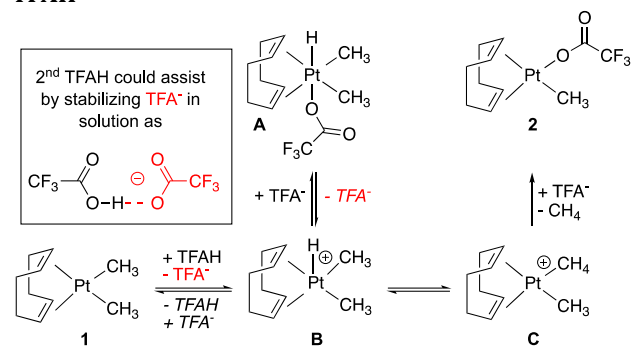
This modified S$_E$(ox) mechanism is consistent with our experimental results that point to a multi-step mechanism involving two equivalents of TFAH. The proposed mechanism can also be used to explain the variable KIE observed. At the lowest reactant concentrations, we imagine that the earlier bimolecular steps in the reaction (formation of **A** and **B**) are slower and thus determine the rate and therefore the KIE. At higher overall reactant concentrations, the earlier steps become faster, a later step (formation of **C**) becomes rate determining. Under these conditions, the observed KIE represents a multiplicative compound effect of KIEs and EIEs from all reaction steps up to and including the rate limiting step.

The possible mechanism presented does not require invocation of proton tunneling to explain the large observed KIE, since the large KIE can now be explained instead by compound effects in a multi-step mechanism. One key piece of experimental data that supports the multi-step pathway is the dependence of KIE on the concentration of reagents. Based on this finding and related work across organometallic chemistry,[16,17,23,38,61,62,64,86–94] we propose that a dilution test be carried out when a large KIE is observed experimentally, to help interpret the large KIE. If the large observed KIE changes when the reaction is diluted, then that is evidence that the large observed KIE does not originate from a single elementary reaction step, and is likely to be a compound effect from multiple steps. This experimental design allowed us to identify a multiple-step pathway in an important system where distinguishing between a single-step and multiple-step pathway had proved challenging, and to show that proton tunneling is not necessary to explain the large KIE.

CONCLUSION

The protonolysis of **1** by TFAH was examined using kinetic measurements over a wide concentration range using stopped-flow and traditional UV-vis spectroscopy, along with ^{1}H NMR studies. We found that the reaction requires two equivalents of acid to reach completion and the rate dependence is second-order in acid, so we conclude that the reaction mechanism involves two molecules of TFAH. We also observed that the KIE is consistently high across several spectroscopic techniques and reaction conditions, with a highest value of 18 ± 3, but it decreases significantly to a low of 5.5 ± 0.9 when the reaction is carried out at lower overall concentration.

Since an elementary reaction would have a constant KIE, we conclude that the reaction mechanism must contain multiple steps.

We suggest one possible mechanism consistent with multiple reaction steps and multiple acid molecules: a modified $S_E(ox)$ pathway, in which oxidative addition of TFAH occurs to generate a Pt(IV) hydride intermediate and a second molecule of TFAH assists in stabilization of the TFA⁻ anion in solution so that a 5-coordinate intermediate can form and undergo reductive elimination (Scheme 3).

We found that the large observed KIE need not be explained by proton tunneling and can instead be explained by a composite of kinetic and equilibrium isotope effects for multiple reaction steps. Indeed, we propose that large KIE values be considered a possible mechanistic indicator of multiple reaction steps occurring before the rate limiting step. A dilution test can be used more generally: if a large observed KIE varies based on reaction concentration, a multi-step mechanism may be responsible.

Overall, we have shown that a simple protonolysis reaction that is a long-studied model for potential methane activation involves more steps and more molecules than previously believed; we suggest one mechanism consistent with these findings. Further, we find that a large KIE can provide mechanistic information by indicating the possibility of multiple reaction steps.

EXPERIMENTAL

General Information

All reagents were purchased from commercial suppliers and used as received unless otherwise noted. The platinum complex **1**, (cod)Pt(Me)$_2$ (78-0700), was purchased from Strem Chemicals, Inc. Anhydrous trifluoroacetic acid (TFAH) (900518) was purchased from Sigma Aldrich. 1,2,3-trimethoxybenzene was purchased from Sigma Aldrich and purified by sublimation. Methylene chloride (CH$_2$Cl$_2$) was dispensed from a Pure Process Technology Solvent Purification System and stored over 3 Å molecular sieves in an amber glass bottle under N$_2$ atmosphere before use. CD$_2$Cl$_2$ (DLM-23-25) and TFAD (DLM-46-10X0.75) were purchased from Cambridge Isotope Laboratories. CD$_2$Cl$_2$ was degassed and stored over activated 3 Å molecular sieves for at least 24 hours before use.

All ^{1}H NMR and UV-vis samples were prepared inside of a VAC Genesis Glovebox under N$_2$ atmosphere. New ampules of TFAD and TFAH were used to prepare the acid stock solutions in all experiments. Aliquots of TFAH or TFAD were added to UV-Vis or NMR samples using a 500-µL gastight syringe from Trajan Scientific and Medical (Cat #: 500R-GT).

^{1}H NMR spectra used for the CH$_4$/CH$_3$D product ratio KIE calculation were collected on a Bruker 600 MHz Avance III spectrometer at 298 K. ^{1}H NMR spectra used in stoichiometry experiments were collected on a 400 MHz Bruker Avance I at 298 K. Spectra were analyzed using the MestReNova software package and chemical shifts were referenced to the residual protio signal of the deuterated solvent.[95]

UV-vis absorption spectra were recorded on an Agilent Cary 60 spectrometer with a Quantum Northwest Versa20/Cary 60 temperature control unit. Constant temperature was maintained at 296 K with a temperature controller. Samples of **1** were prepared in gastight screw-cap 3.5-mL quartz cells with an optical pathlength of 1 cm obtained from Starna Cells, Inc. (GL14-C).

^{1}H NMR KIE experiments. Stock solutions for KIE product ratio experiments were prepared as follows. (i) Stock solution of compound **1** (50 mM) was prepared by dissolving **1** (84 mg, 0.25 mmol) in CD$_2$Cl$_2$ in a 5-mL volumetric flask; (ii) TFAD/TFAH (10:1 v/v) stock solution was prepared by combining 900 µL of TFAD with 90 µL of TFAH; (iii) TFAD/TFAH (1:1 v/v, 1.3 M) was prepared as follows: two separate 2.6 M stock solutions of TFAD and TFAH were prepared by diluting 200 µL of neat TFAD or TFAH with CD$_2$Cl$_2$ in a 1-mL volumetric flask. An aliquot (500 µL) of TFAH stock solution (2.6 M) was combined with a corresponding aliquot (500 µL) of TFAD stock solution (2.6 M).

Complex **1** (0.015 mmol, 300 µL aliquot of 50 mM stock solution in CD$_2$Cl$_2$) was added to a 5 mm NMR tube, then diluted with 400 µL of additional CD$_2$Cl$_2$. The tube was capped with a rubber septum, taken out of the glovebox, and allowed to equilibrate for 5 min in a 297 K water bath. A 500-µL gas-tight syringe was used to add TFAD/TFAH stock solution (200 µL) dropwise to the NMR sample with occasional shaking to mix. Immediately after the addition of acid solution, five single-scan spectra were collected with a delay time of 180 seconds between scans. Each experiment was performed in triplicate. The relative integration of the CH$_3$D and CH$_4$ signals were used to calculate the KIE. Below is an example calculation for KIE determination using 10:1 TFAD:TFAH.

$$KIE = \frac{\frac{10}{4} \times (\int CH_4)}{\frac{1}{3} \times (\int CH_3D)} = \frac{\frac{10}{4} \times (1.28)}{\frac{1}{3} \times (0.79)} = \frac{3.20}{0.26} = 12.3$$

^{1}H NMR stoichiometry experiments. Complex **1** (35 mg, 0.1 mmol) was dissolved in CD$_2$Cl$_2$ in a 1 mL volumetric flask to generate a stock solution of **1** (0.1 M). 1,2,3-trimethoxybenzene (TMB) (17 mg, 0.1 mmol) as an internal standard was dissolved in CD$_2$Cl$_2$ in a 1 mL volumetric flask to generate a stock solution of TMB (0.1 M). Samples were prepared by adding an aliquot of **1** stock (90 µL) and an aliquot of TMB stock (90 µL) each to 5 separate PTFE-stoppered NMR tubes and diluting each with CD$_2$Cl$_2$ to a total volume of 450 µL (0.02 M). Samples were removed from the glovebox and ^{1}H NMR spectra were collected to quantify the initial concentration of **1** for each sample. The tubes were then returned to the glovebox, and TFAH was added (0.0, 0.5, 1.0, 2.0, or 100 equiv from a 0.2 M stock solution in CD$_2$Cl$_2$). All tubes were inverted a minimum of three times to ensure mixing and ^{1}H NMR spectra were obtained of each sample immediately. The samples were then allowed to stand in the glovebox for 72 h and additional spectra were collected. Every 24 h the tubes were inverted an additional three times.

*Molar extinction coefficients for **1**.* In the glovebox, a stock solution of **1** (35 mg, 0.1 mmol) was prepared with CH_2Cl_2 in a 1 mL volumetric flask (0.1 M). A 10 μL aliquot of the stock solution was added to 3 mL of CH_2Cl_2 in a quartz cuvette. The solution was removed from the glovebox and stirred at 1500 rpm for 2 minutes before collecting the absorbance spectrum from 200-400 nm. The cuvette was then returned to the glovebox, another 10 μL aliquot was added, removed from the glovebox, and the absorbance collected. This was repeated through 50 μL of **1** stock added in total. Local absorbance maxima for **1** were determined to be λ_{max} = 288, 318, 358 nm. Molar extinction coefficients at each λ_{max} were calculated from the slope of the absorbance maxima versus the concentration of **1** collected from triplicate experiments.

UV-Vis KIE Experiments. Solutions of complex **1** were prepared as follows: Complex **1** (20 mg, 0.06 mmol) was dissolved in CH_2Cl_2 (1 mL) to generate a stock solution of **1** (0.06 M). (i) 80 μL of the stock solution was added to a blanked cuvette containing 2870 μL CH_2Cl_2 to generate a final solution of concentration 1.6 mM, and (ii) 20 μL of the stock solution was added to a blanked cuvette containing 2930 μL CH_2Cl_2 to generate a final solution of concentration 0.4 mM. Complex **1** (20 mg, 0.06 mmol) was dissolved in CH_2Cl_2 (10 mL) to generate a second stock solution of **1** (0.006 M). 50 μL of this stock was added to a blanked cuvette containing 2900 μL CH_2Cl_2 to generate a final solution of concentration 0.1 mM. Concentrations of all final solutions of complex **1** were quantified using UV-vis spectroscopy prior to the addition of TFAH or TFAD.

Solutions of acids were prepared as follows: stock solutions of TFAH or TFAD (1 M) were prepared by diluting 77 μL of neat TFAH or TFAD with CH_2Cl_2 in a 1 mL volumetric flask. (i) a 191 μL aliquot of the 1 M stock was diluted with CH_2Cl_2 in a 1 mL volumetric flask to generate a working solution of TFAH or TFAD (0.2 M). An aliquot (50 μL) of the TFAH or TFAD working solution (0.2 M) was added to the cuvette containing **1** and 2950 μL of CH_2Cl_2 to give a final concentration of 3.2 mM TFAH or TFAD. (ii) a 48 μL aliquot of the 1 M stock was diluted with CH_2Cl_2 in a 1 mL volumetric flask to generate a working solution TFAH or TFAD (0.05 M). A 50 μL aliquot of the working solution of TFAH or TFAD (0.05 M) was added to the cuvette containing **1** and 2950 μL of CH_2Cl_2 to give a final concentration of 0.8 mM TFAH or TFAD. (iii) a 60 μL aliquot of the 1 M stock was diluted with CH_2Cl_2 in a 5 mL volumetric flask to generate a working solution of TFAH or TFAD (0.01 M). An aliquot (50 μL) of the TFAH or TFAD working solution (0.01 M) was added to the cuvette containing **1** and 2950 μL of CH_2Cl_2 to give a final concentration of 0.2 mM TFAH or TFAD. Following the addition of acid, protonolysis and deuterolysis reactions were monitored at 0.5-second intervals until the slope of the decay curve had plateaued (5-500 minutes) with a scan rate of 9600 nm/min between 200-400 nm for full scans or at 288 nm, 318 nm, or 358 nm for kinetic data acquisition. The reaction mixture was stirred at 1800 rpm throughout the experiment.

Rate calculations. Observed rate constants for the protonolysis $(k(obs)_H)$ and deuterolysis $(k(obs)_D)$ reaction of **1** with TFAH and TFAD were calculated by the method of initial rates, by pseudo-first-order fitting, or both. For the method of initial rates, the slope of a plot of absorbance versus time was measured for the first 9% reaction conversion. Pseudo-first-order observed rate constants were determined from nonlinear least-squares fitting of the absorbance versus time profiles to a single exponential decay equation.[59] The "GRG Nonlinear" method within the SOLVER function in Excel software was used with convergence value of 0.000001. KIEs were calculated from an average of triplicate $k(obs)_H$ and $k(obs)_D$ values.[96,97]

Stopped-flow UV-vis spectroscopy

Sample preparation: Stock solutions of compound **1** (3.2 mM) were prepared by dissolving compound **1** (10.7 mg) in CH_2Cl_2 (10.0 mL). Stock solutions of TFAH and TFAD (0.108, 0.320, 0.800, 1.200 M) were prepared by diluting neat TFAH (41.5, 122.5, 306.0, or 459.0 μL) or neat TFA-d_1 (41.9, 123.5, 309.0, or 463.0 μL) to 5.00 mL with CH_2Cl_2 in a volumetric flask. Stock solutions were loaded into syringes (Hamilton 1000 series, gas-tight) with rubber septa over the ends and carried from the glovebox to the stopped-flow spectrophotometer in sealed Ziploc bags immediately after they were prepared.

Data acquisition: Stopped-flow data were collected using an Applied Photophysics SX-20 stopped-flow UV-vis spectrometer equipped with a removable 20 μL quartz cell and a photodiode array detector. Measurements were acquired at ambient lab temperature (294 K). The stopped flow apparatus was rinsed thoroughly with dry, degassed CH_2Cl_2 before use; nitrogen gas flowed through the apparatus throughout the experiments. Equal-volume injections were made of the stock solutions of **1** and of acid for rapid mixing in the cell. For each sample syringe, the apparatus was rinsed with at least four injections of sample before three separate injections were used to collect the reported data in triplicate. This entire procedure was repeated in triplicate to produce a final set of data as a triplicate of triplicates for each of the eight experimental conditions.

UV-visible absorbance data were collected using an optical pathlength of 2 mm over a wavelength range from 180 to 730 nm. Data were collected every 1 ms for a time period sufficient to observe complete decay (0.5 to 40 sec). The absorbance values at 318 nm over time were fit to a single exponential using the SX Pro-Data software version 2.5.1852 (Applied Photophysics) to extract observed rate constants.

Computational Details

Calculations were completed using the Extreme Science and Engineering Discovery Environment (XSEDE)[98] Bridges-2 at the Pittsburgh Computing Center (PSC) with Gaussian16[99] suite of programs, and results were visualized using GaussView06[100]. The structures were optimized to a minima using the B3LYP[101–103] level of theory with a split basis set (def2svpp[104–107] for all light atoms, def2tzvpp[104–107] for Pt). Gibbs free energies were obtained from thermally corrected energy values from the frequency calculations on minimized structures.

ASSOCIATED CONTENT

Supporting Information

AUTHOR INFORMATION

Corresponding Author

* mbowring@reed.edu

Author Contributions

The manuscript was written through contributions of all authors. All authors have given approval to the final version of the manuscript.

Notes

The authors declare no competing financial interests.

ACKNOWLEDGMENTS

ABBREVIATIONS

cod, 1,5-cyclooctadiene; dfepe, $(C_2F_5)_2PCH_2CH_2P(C_2F_5)_2$; KIE, kinetic isotope effect; TFAH, trifluoroacetic acid; TFAD, deuterated trifluoroacetic acid; TFA⁻, trifluoroacetate anion; tmeda, *N,N,N′,N′*-tetramethylethylenediamine

REFERENCES

(1)   Caballero, A.; Pérez, P. J. Methane as Raw Material in Synthetic Chemistry: The Final Frontier. *Chem. Soc. Rev.* **2013**, *42* (23), 8809–8820. https://doi.org/10.1039/C3CS60120J.

(2)   Gunsalus, N. J.; Koppaka, A.; Park, S. H.; Bischof, S. M.; Hashiguchi, B. G.; Periana, R. A. Homogeneous Functionalization of Methane. *Chem. Rev.* **2017**, *117* (13), 8521–8573. https://doi.org/10.1021/acs.chemrev.6b00739.

(3)   Schwarz, H. Chemistry with Methane: Concepts Rather than Recipes. *Angew. Chem., Int. Ed.* **2011**, *50* (43), 10096–10115. https://doi.org/10.1002/anie.201006424.

(4)   Arndtsen, B. A.; Bergman, R. G.; Mobley, T. A.; Peterson, T. H. Selective Intermolecular Carbon-Hydrogen Bond Activation by Synthetic Metal Complexes in Homogeneous Solution. *Acc. Chem. Res.* **1995**, *28* (3), 154–162.

(5)   Altus, K. M.; Love, J. A. The Continuum of Carbon–Hydrogen (C–H) Activation Mechanisms and Terminology. *Commun. Chem.* **2021**, *4* (1), 173. https://doi.org/10.1038/s42004-021-00611-1.

(6)   Goldberg, K. I.; Goldman, A. S. Large-Scale Selective Functionalization of Alkanes. *Acc. Chem. Res.* **2017**, *50* (3), 620–626. https://doi.org/10.1021/acs.accounts.6b00621.

(7)   Labinger, J. A.; Bercaw, J. E. Understanding and Exploiting C–H Bond Activation. *Nature* **2002**, *417* (6888), 507–514. https://doi.org/10.1038/417507a.

(8)   Olivos-Suarez, A. I.; Szécsényi, À.; Hensen, E. J. M.; Ruiz-Martinez, J.; Pidko, E. A.; Gascon, J. Strategies for the Direct Catalytic Valorization of Methane Using Heterogeneous Catalysis: Challenges and Opportunities. *ACS Catal.* **2016**, *6* (5), 2965–2981. https://doi.org/10.1021/acscatal.6b00428.

(9)   Periana, R. A.; Taube, D. J.; Gamble, S.; Taube, H.; Satoh, T.; Fujii, H. Platinum Catalysts for the High-Yield Oxidation of Methane to a Methanol Derivative. *Science* **1998**, *280* (5363), 560–564. https://doi.org/10.1126/science.280.5363.560.

(10)   Shilov, A. E.; Shul'pin, G. B. Activation of C–H Bonds by Metal Complexes. *Chem. Rev.* **1997**, *97* (8), 2879–2932.

(11)   Palkovits, R.; von Malotki, C.; Baumgarten, M.; Müllen, K.; Baltes, C.; Antonietti, M.; Kuhn, P.; Weber, J.; Thomas, A.; Schüth, F. Development of Molecular and Solid Catalysts for the Direct Low-Temperature Oxidation of Methane to Methanol. *ChemSusChem* **2010**, *3* (2), 277–282. https://doi.org/10.1002/cssc.200900123.

(12)   Stahl, S. S.; Labinger, J. A.; Bercaw, J. E. Homogeneous Oxidation of Alkanes by Electrophilic Late Transition Metals. *Angew. Chem., Int. Ed.* **1998**, *37* (16), 2180–2192. https://doi.org/10.1002/(SICI)1521-3773(19980904)37:16<2180::AID-ANIE2180>3.0.CO;2-A.

(13)   Lersch, M.; Tilset, M. Mechanistic Aspects of C–H Activation by Pt Complexes. *Chem. Rev.* **2005**, *105* (6), 2471–2526. https://doi.org/10.1021/cr030710y.

(14)   Ahrens, S.; Strassner, T. Detour-Free Synthesis of Platinum-Bis-NHC Chloride Complexes, Their Structure and Catalytic Activity in the CH Activation of Methane. *Inorg. Chim. Acta* **2006**, *359* (15), 4789–4796. https://doi.org/10.1016/j.ica.2006.05.042.

(15)   Labinger, J. A. Platinum-Catalyzed C–H Functionalization. *Chem. Rev.* **2017**, *117* (13), 8483–8496. https://doi.org/10.1021/acs.chemrev.6b00583.

(16)   Stahl, S. S.; Labinger, J. A.; Bercaw, J. E. Exploring the Mechanism of Aqueous C–H Activation by Pt(II) through Model Chemistry: Evidence for the Intermediacy of Alkylhydridoplatinum(IV) and Alkane σ-Adducts. *J. Am. Chem. Soc.* **1996**, *118* (25), 5961–5976. https://doi.org/10.1021/ja960110z.

(17)   Romeo, R.; D'Amico, G. Mechanistic Insight into the Protonolysis of the Pt–C Bond as a Model for C–H Bond Activation by Platinum(II) Complexes. *Organometallics* **2006**, *25* (14), 3435–3446. https://doi.org/10.1021/om060217n.

(18)   Bercaw, J. E.; Chen, G. S.; Labinger, J. A.; Lin, B.-L. Hydrogen Tunneling in Protonolysis of Platinum(II) and Palladium(II) Methyl Complexes: Mechanistic Implications. *J. Am. Chem. Soc.* **2008**, *130* (52), 17654–17655.

(19)   Bercaw, J. E.; Chen, G. S.; Labinger, J. A.; Lin, B.-L. Protonolysis of Platinum(II) and Palladium(II) Methyl Complexes: A Combined Experimental and Theoretical Investigation. *Organometallics* **2010**, *29* (19), 4354–4359. https://doi.org/10.1021/om100655w.

(20)   Scott, V. J.; Labinger, J. A.; Bercaw, J. E. Large Kinetic Isotope Effects for the Protonolysis of Metal–Methyl Complexes Are Not Reliable Mechanistic Indicators. *Organometallics* **2011**, *30* (16), 4374–4378. https://doi.org/10.1021/om200432b.

(21)   Hill, G. S.; Rendina, L. M.; Puddephatt, R. J. Alkyl(Hydrido)Platinum(IV) Complexes: The Mechanism of Pt-C

Bond Protonolysis. *Organometallics* **1995**, *14* (10), 4966–4968. https://doi.org/10.1021/om00010a073.

(22) Hinman, J. G.; Baar, C. R.; Jennings, M. C.; Puddephatt, R. J. Protonolysis of Dimethylplatinum(II) Complexes: Primary Attack at Metal or Ligand. *Organometallics* **2000**, *19* (4), 563–570. https://doi.org/10.1021/om990840q.

(23) Bennett, B. L.; Hoerter, J. M.; Houlis, J. F.; Roddick, D. M. Metal–Alkyl Bond Protonolysis Studies of (Dfepe)Pt(Me)X Complexes in Acidic Media. *Organometallics* **2000**, *19* (4), 615–621. https://doi.org/10.1021/om990743x.

(24) Wik, B. J.; Ivanovic-Burmazovic, I.; Tilset, M.; van Eldik, R. Mechanistic Information from Low-Temperature Rapid-Scan and NMR Measurements on the Protonation and Subsequent Reductive Elimination Reaction of a (Diimine)Platinum(II) Dimethyl Complex. *Inorg. Chem.* **2006**, *45* (9), 3613–3621. https://doi.org/10.1021/ic0519537.

(25) Ong, C. M.; Burchell, T. J.; Puddephatt, R. J. Activation of Si–C or C–H Bonds in Tetramethylsilane: Evidence from Protonolysis of (Trimethylsilyl)Methyl–Platinum Bonds. *Organometallics* **2004**, *23* (7), 1493–1495. https://doi.org/10.1021/om0400088.

(26) Holtcamp, M. W.; Labinger, J. A.; Bercaw, J. E. Ligand Effects on the Rates of Protonolysis and Isotopic Exchange for Platinum(II) Alkyls. *Inorg. Chim. Acta* **1997**, *265* (1–2), 117–125. https://doi.org/10.1016/S0020-1693(97)05675-2.

(27) Behnia, A.; Fard, M. A.; Blacquiere, J. M.; Puddephatt, R. J. Mild and Selective Pd–Ar Protonolysis and C–H Activation Promoted by a Ligand Aryloxide Group. *Dalton Trans.* **2018**, *47* (10), 3538–3548.

(28) Johansson, L.; Ryan, O. B.; Rømming, C.; Tilset, M. Unexpected Selectivities in C–H Activations of Toluene and *p*-Xylene at Cationic Platinum(II) Diimine Complexes. New Mechanistic Insight into Product-Determining Factors. *J. Am. Chem. Soc.* **2001**, *123* (27), 6579–6590. https://doi.org/10.1021/ja010277e.

(29) Procelewska, J.; Zahl, A.; van Eldik, R.; Zhong, H. A.; Labinger, J. A.; Bercaw, J. E. Activation Volume Measurement for C–H Activation. Evidence for Associative Benzene Substitution at a Platinum(II) Center. *Inorg. Chem.* **2002**, *41* (11), 2808–2810. https://doi.org/10.1021/ic0201710.

(30) Dong, D.; Slack, D. A.; Baird, M. C. Stereochemistry and Mechanisms of Mercury(II) Chloride Cleavage of Three -1,2-Dideuteriophenethyl Compounds of Iron, Manganese, and Tungsten. *Inorg. Chem.* **1979**, *18* (1), 188–191.

(31) Fard, M. A.; Behnia, A.; Puddephatt, R. J. Cycloneophylplatinum Chemistry: A New Route to Platinum(II) Complexes and the Mechanism and Selectivity of Protonolysis of Platinum–Carbon Bonds. *Organometallics* **2018**, *37* (19), 3368–3377. https://doi.org/10.1021/acs.organomet.8b00650.

(32) Wik, B. J.; Lersch, M.; Tilset, M. The Metal Is the Kinetic Site of Protonation of (Diimine)Pt Dimethyl Complexes. *J. Am. Chem. Soc.* **2002**, *124* (41), 12116–12117. https://doi.org/10.1021/ja027649j.

(33) Jawad, J. K.; Puddephatt, R. J.; Stalteri, M. A. Selectivity in Reactions of Alkyl-Aryl-Transition-Metal Complexes with Electrophiles. *Inorg. Chem.* **1982**, *21* (1), 332–337. https://doi.org/10.1021/ic00131a061.

(34) De Felice, V.; De Renzi, A.; Panunzi, A.; Tesauro, D. Cis-(Hydrido)Hydrocarbylplatinum(IV) Complexes as Intermediates in the PtII-C Bond Breaking. *J. Organomet. Chem.* **1995**, *488* (1), C13–C14. https://doi.org/10.1016/0022-328X(94)00038-E.

(35) Stahl, S. S.; Labinger, J. A.; Bercaw, J. E. Formation and Reductive Elimination of a Hydridoalkylplatinum(IV) Intermediate upon Protonolysis of an Alkylplatinum(II) Complex. *J. Am. Chem. Soc.* **1995**, *117* (36), 9371–9372. https://doi.org/10.1021/ja00141a037.

(36) Truong, P. T.; Miller, S. G.; McLaughlin Sta. Maria, E. J.; Bowring, M. A. Large Isotope Effects in Organometallic Chemistry. *Chem. - Eur. J.* **2021**, *27* (60), 14800–14815. https://doi.org/10.1002/chem.202102189.

(37) Simmons, E. M.; Hartwig, J. F. On the Interpretation of Deuterium Kinetic Isotope Effects in C–H Bond Functionalizations by Transition-Metal Complexes. *Angew. Chem., Int. Ed.* **2012**, *51* (13), 3066–3072. https://doi.org/10.1002/anie.201107334.

(38) Jones, W. D. Isotope Effects in C–H Bond Activation Reactions by Transition Metals. *Acc. Chem. Res.* **2003**, *36* (2), 140–146. https://doi.org/10.1021/ar020148i.

(39) Lloyd-Jones, G. C.; Muñoz, M. P. Isotopic Labelling in the Study of Organic and Organometallic Mechanism and Structure: An Account. *J. Label. Compd. Radiopharm.* **2007**, *50* (11–12), 1072–1087. https://doi.org/10.1002/jlcr.1382.

(40) Parkin, G. Temperature-Dependent Transitions Between Normal and Inverse Isotope Effects Pertaining to the Interaction of H–H and C–H Bonds with Transition Metal Centers. *Acc. Chem. Res.* **2009**, *42* (2), 315–325. https://doi.org/10.1021/ar800156h.

(41) Gómez-Gallego, M.; Sierra, M. A. Kinetic Isotope Effects in the Study of Organometallic Reaction Mechanisms. *Chem. Rev.* **2011**, *111* (8), 4857–4963. https://doi.org/10.1021/cr100436k.

(42) Slaughter, L. M.; Wolczanski, P. T.; Klinckman, T. R.; Cundari, T. R. Inter- and Intramolecular Experimental and Calculated Equilibrium Isotope Effects for (Silox)$_2$(^{t}Bu$_3$SiND)TiR + RH (Silox = ^{t}Bu$_3$SiO): Inferred Kinetic Isotope Effects for RH/D Addition to Transient (Silox)$_2$TiNSi^{t}Bu$_3$. *J. Am. Chem. Soc.* **2000**, *122* (33), 7953–7975.

(43) Bell, R. *The Tunnel Effect in Chemistry*; Chapman and Hall: Boca Raton, FL, 1980.

(44) Melander, L.; Saunders, W. H. *Reaction Rates of Isotopic Molecules*; Wiley, 1980.

(45) Fukuzumi, S.; Lee, Y.-M.; Nam, W. Deuterium Kinetic Isotope Effects as Redox Mechanistic Criterions. *Bull. Korean Chem. Soc.* **2021**, *42* (12), 1558–1568. https://doi.org/10.1002/bkcs.12417.

(46) Wu, A.; Mayer, J. M. Hydrogen Atom Transfer Reactions of a Ruthenium Imidazole Complex: Hydrogen Tunneling and the Applicability of the Marcus Cross Relation. *J. Am. Chem. Soc.* **2008**, *130* (44), 14745–14754.

(47) Romeo, R.; Minniti, D.; Lanza, S.; Uguagliati, P.; Belluco, U. Mechanism of Electrophilic Cleavage of the Platinum-Carbon Bond in Platinum(II)-Diaryl Complexes. *Inorg. Chem.* **1978**, *17* (10), 2813–2818. https://doi.org/10.1021/ic50188a026.

(48) Romeo, R.; Minniti, D.; Lanza, S. Mechanism of Electrophilic Cleavage of the Pt-C (Alkyl) Bond in Trans-[Pt(PEt3)2 (YC6H4)(CH3)] Complexes. *J. Organomet. Chem.* **1979**, *165* (2), C36–C38. https://doi.org/10.1016/S0022-328X(00)94333-X.

(49) Alibrandi, G.; Minniti, D.; Monsu Scolaro, L.; Romeo, R. Selective Cleavage of the Platinum-Carbon(Alkyl) Bond in Alkylarylplatinum(II) Complexes and Mechanism of Cis to Trans Isomerization of the Resulting Solvento Complexes. *Inorg. Chem.* **1988**, *27* (2), 318–324. https://doi.org/10.1021/ic00275a019.

(50) Romeo, R.; Plutino, M. R.; Elding, L. I. Protonolysis of Dialkyl- and Alkylarylplatinum(II) Complexes and Geometrical Isomerization of the Derived Monoorgano–Solvento Complexes: Clear-Cut Examples of Associative and Dissociative Pathways in Platinum(II) Chemistry. *Inorg. Chem.* **1997**, *36* (25), 5909–5916. https://doi.org/10.1021/ic9704905.

(51) Bennett, B. L.; Birnbaum, J.; Roddick, D. M. Protonation Studies of Electrophilic Platinum(II) Alkyl Complexes: Synthesis and Characterization of (Dfepe)Pt(Me)X (X = O2CCF3, OSO2CF3, OSO3H). *Polyhedron* **1995**, *14* (1), 187–195. https://doi.org/10.1016/0277-5387(94)00366-M.

(52) Kalberer, E. W.; Houlis, J. F.; Roddick, D. M. Protolytic Stability of (Dfepe)Pt(Ph)O$_2$CCF$_3$: Supporting Evidence for a Concerted S$_E$2 Protonolysis Mechanism. *Organometallics* **2004**, *23* (17), 4112–4115. https://doi.org/10.1021/om049682f.

(53) Parmene, J.; Ivanović-Burmazović, I.; Tilset, M.; van Eldik, R. Combined Low Temperature Rapid Scan and 1H NMR

Mechanistic Study of the Protonation and Subsequent Benzene Elimination from a (Diimine)Platinum(II) Diphenyl Complex Relevant to Arene C–H Activation. *Inorg. Chem.* **2009**, *48* (19), 9092–9103. https://doi.org/10.1021/ic9005746.

(54) We found an arithmetic error in the reports by Bercaw et al., which was confirmed by email correspondence with the authors. The reported KIE values can each be multiplied by a factor of 3/4 to generate the correct values.

(55) Mai, B. K.; Kim, Y. Kinetic Isotope Effects as a Probe for the Protonolysis Mechanism of Alkylmetal Complexes: VTST/MT Calculations Based on DFT Potential Energy Surfaces. *Inorg. Chem.* **2016**, *55* (19), 9822–9829. https://doi.org/10.1021/acs.inorgchem.6b01614.

(56) Mazzone, G.; Russo, N.; Sicilia, E. Dimethylplatinum(II) Complexes: Computational Insights into Pt–C Bond Protonolysis. *Inorg. Chem.* **2011**, *50* (20), 10091–10101. https://doi.org/10.1021/ic201004n.

(57) Klein, A.; van Slageren, J.; Záliš, S. Spectroscopy and Photochemical Reactivity of Cyclooctadiene Platinum Complexes. *Journal of Organometallic Chemistry* **2001**, *620* (1–2), 202–210. https://doi.org/10.1016/S0022-328X(00)00792-0.

(58) Liu, H.; Brewer, C. R.; Walker, A. V.; McElwee-White, L. Photochemistry of 1,5-Cyclooctadiene Platinum Complexes for Photoassisted Chemical Vapor Deposition. *Organometallics* **2020**, *39* (24), 4565–4574. https://doi.org/10.1021/acs.organomet.0c00616.

(59) Habibzadeh, S.; Rashidi, M.; Nabavizadeh, S. M.; Mahmoodi, L.; Hosseini, F. N.; Puddephatt, R. J. Steric and Solvent Effects on the Secondary Kinetic α-Deuterium Isotope Effects in the Reaction of Methyl Iodide with Organoplatinum(II) Complexes: Application of a Second-Order Technique in Measuring the Rates of Rapid Processes. *Organometallics* **2010**, *29* (1), 82–88. https://doi.org/10.1021/om900778u.

(60) Wolczanski, P. T. Activation of Carbon–Hydrogen Bonds via 1,2-RH-Addition/-Elimination to Early Transition Metal Imides. *Organometallics* **2018**, *37* (4), 505–516. https://doi.org/10.1021/acs.organomet.7b00753.

(61) Wang, D.; Izawa, Y.; Stahl, S. S. Pd-Catalyzed Aerobic Oxidative Coupling of Arenes: Evidence for Transmetalation between Two Pd(II)-Aryl Intermediates. *J. Am. Chem. Soc.* **2014**, *136* (28), 9914–9917.

(62) Lloyd-Jones, G. C.; Slatford, P. A. Unusually Large Primary ^{2} H/ ^{1} H Kinetic Isotope Effects Accompanying a *Syn* -β-H Elimination Reaction in a σ-Alkyl–Palladium Complex. *J. Am. Chem. Soc.* **2004**, *126* (9), 2690–2691. https://doi.org/10.1021/ja039349n.

(63) Mao, Z.; Campbell, C. T. Kinetic Isotope Effects: Interpretation and Prediction Using Degrees of Rate Control. *ACS Catal.* **2020**, *10* (7), 4181–4192. https://doi.org/10.1021/acscatal.9b05637.

(64) Anderson, D. R.; Faibish, N. C.; Beak, P. Complex-Induced Proximity Effects in Directed Lithiations: Analysis of Intra- and Intermolecular Kinetic Isotope Effects in Directed Aryl and Benzylic Lithiations. *J. Am. Chem. Soc.* **1999**, *121* (33), 7553–7558. https://doi.org/10.1021/ja991043m.

(65) Hwang, C. C.; Grissom, C. B. Unusually Large Deuterium Isotope Effects in Soybean Lipoxygenase Are Not Caused by a Magnetic Isotope Effect. *J. Am. Chem. Soc.* **1994**, *116* (2), 795–796. https://doi.org/10.1021/ja00081a061.

(66) Janak, K. E.; Churchill, D. G.; Parkin, G. Kinetic and Equilibrium Deuterium Isotope Effects for C–H Bond Reductive Elimination and Oxidative Addition Reactions Involving the Ansa–Tungstenocene Methyl–Hydride Complex [Me2Si(C5Me4)2]W(Me)H. In *Activation and Functionalization of C-H Bonds*; Goldberg, K. I., Goldman, A. S., Eds.; ACS Symposium Series; American Chemical Society, 2004; Vol. 885, pp 86–204.

(67) Świderek, K.; Paneth, P. Binding Isotope Effects. *Chem. Rev.* **2013**, *113* (10), 7851–7879. https://doi.org/10.1021/cr300515x.

(68) Fekl, U.; Goldberg, K. I. Homogeneous Hydrocarbon C-H Bond Activation and Functionalization. In *Advances in Inorganic Chemistry*; Solvent Exchange on Metal Ions; Academic Press, 2003; Vol. 54, pp 259–320. https://doi.org/10.1016/S0898-8838(03)54005-3.

(69) Bartlett, K. L.; Goldberg, K. I.; Borden, W. T. A Computational Study of Reductive Elimination Reactions to Form C–H Bonds from Pt(II) and Pt(IV) Centers. Why Does Ligand Loss Precede Reductive Elimination from Six-Coordinate but Not Four-Coordinate Platinum? *J. Am. Chem. Soc.* **2000**, *122* (7), 1456–1465. https://doi.org/10.1021/ja9915706.

(70) Bartlett, K. L.; Goldberg, K. I.; Borden, W. T. Computational Study of Reductive Elimination Reactions to Form C–H Bonds from Platinum(II) and Platinum(IV) Centers with Strongly Coordinating Trimethylphosphine Ligands. *Organometallics* **2001**, *20* (13), 2669–2678. https://doi.org/10.1021/om010072e.

(71) Hartwig, John F. *Organotransition Metal Chemistry: From Bonding to Catalysis*; University Science Books: Mill Valley, CA, 2010.

(72) Brown, M. P.; Puddephatt, R. J.; Upton, C. E. E. Mechanism of Reductive Elimination of Ethane from Some Halogenotrimethylbis(Tertiary Phosphine)Platinum(IV) Complexes. *J. Chem. Soc., Dalton Trans.* **1974**, No. 22, 2457. https://doi.org/10.1039/dt9740002457.

(73) Goldberg, K. I.; Yan, J.; Breitung, E. M. Energetics and Mechanisms of Carbon-Carbon and Carbon-Iodide Reductive Elimination from a Pt(IV) Center. *J. Am. Chem. Soc.* **1995**, *117* (26), 6889–6896. https://doi.org/10.1021/ja00131a010.

(74) Crumpton, D. M.; Goldberg, K. I. Five-Coordinate Intermediates in Carbon–Carbon Reductive Elimination Reactions from Pt(IV). *J. Am. Chem. Soc.* **2000**, *122* (5), 962–963. https://doi.org/10.1021/ja9912123.

(75) Williams, B. S.; Holland, A. W.; Goldberg, K. I. Direct Observation of C–O Reductive Elimination from Pt(IV). *J. Am. Chem. Soc.* **1999**, *121* (1), 252–253. https://doi.org/10.1021/ja982211y.

(76) Meot-Ner, M.; Elmore, D. E.; Scheiner, S. Ionic Hydrogen Bond Effects on the Acidities, Basicities, Solvation, Solvent Bridging, and Self-Assembly of Carboxylic Groups. *J. Am. Chem. Soc.* **1999**, *121* (33), 7625–7635. https://doi.org/10.1021/ja982173i.

(77) Fourmond, V.; Jacques, P.-A.; Fontecave, M.; Artero, V. H $_2$ Evolution and Molecular Electrocatalysts: Determination of Overpotentials and Effect of Homoconjugation. *Inorg. Chem.* **2010**, *49* (22), 10338–10347. https://doi.org/10.1021/ic101187v.

(78) Guo, J.; Tolstoy, P. M.; Koeppe, B.; Golubev, N. S.; Denisov, G. S.; Smirnov, S. N.; Limbach, H.-H. Hydrogen Bond Geometries and Proton Tautomerism of Homoconjugated Anions of Carboxylic Acids Studied via H/D Isotope Effects on 13C NMR Chemical Shifts. *J. Phys. Chem. A* **2012**, *116*, 11180–11188. https://doi.org/10.1021/jp304943h.

(79) Appel, A. M.; Helm, M. L. Determining the Overpotential for a Molecular Electrocatalyst. *ACS Catal.* **2014**, *4*, 630–633. https://doi.org/10.1021/cs401013v.

(80) Roberts, J. M.; Belowich, M. E.; Peterson, T. H.; Bellinger, E.; Syverud, K.; Laitar, D. S.; Sidle, T. Homoconjugated Acids as Low Cyclosiloxane-Producing Silanol Polycondensation Catalysts. *ACS Omega* **2020**, *5* (38), 24954–24963. https://doi.org/10.1021/acsomega.0c03883.

(81) McCarthy, B. D.; Martin, D. J.; Rountree, E. S.; Ullman, A. C.; Dempsey, J. L. Electrochemical Reduction of Brønsted Acids by Glassy Carbon in Acetonitrile - Implications for Electrocatalytic Hydrogen Evolution. *Inorg. Chem.* **2014**, *53*, 8350–8361. https://doi.org/10.1021/ic500770k.

(82) Rountree, E. S.; Dempsey, J. L. Reactivity of Proton Sources with a Nickel Hydride Complex in Acetonitrile: Implications for the Study of Fuel-Forming Catalysts. *Inorg. Chem.* **2016**, *55*, 5079–5087. https://doi.org/10.1021/acs.inorgchem.6b00885.

(83) Stratakes, B. M.; Dempsey, J. L.; Miller, A. J. M. Determining the Overpotential of Electrochemical Fuel Synthesis Mediated by Molecular Catalysts: Recommended Practices, Standard Reduction Potentials, and Challenges. *ChemElectroChem* **2021**, *8* (22), 4161–4180. https://doi.org/10.1002/celc.202100576.

(84) Williams, B. S.; Goldberg, K. I. Studies of Reductive Elimination Reactions To Form Carbon–Oxygen Bonds from Pt(IV) Complexes. *J. Am. Chem. Soc.* **2001**, *123* (11), 2576–2587. https://doi.org/10.1021/ja003366k.

(85) Smit, J. B. M.; Marais, C.; Malan, F. P.; Bezuidenhout, B. C. B. Crystal Structure of (2,4-Dimethoxybenzyl)Triphenylphosphonium Trifluoroacetate — Trifluoroacetic Acid (1/1), C31H27F6O6P. *Z. Kristallogr. - New Cryst. Struct.* **2019**, *234* (4), 621–623. https://doi.org/10.1515/ncrs-2018-0573.

(86) Hammarback, L. A.; Aucott, B. J.; Bray, J. T. W.; Clark, I. P.; Towrie, M.; Robinson, A.; Fairlamb, I. J. S.; Lynam, J. M. Direct Observation of the Microscopic Reverse of the Ubiquitous Concerted Metalation Deprotonation Step in C–H Bond Activation Catalysis. *J. Am. Chem. Soc.* **2021**, *143* (3), 1356–1364. https://doi.org/10.1021/jacs.0c10409.

(87) Beckers, I.; Henrion, M.; Vos, D. E. D. The Dual Effect of the Acetate Ligand on the Mechanism of the Pd-Catalyzed C–H/C–H Coupling of Benzene. *ChemCatChem* **2020**, *12* (1), 90–94. https://doi.org/10.1002/cctc.201901238.

(88) Guimond, N.; Gorelsky, S. I.; Fagnou, K. Rhodium(III)-Catalyzed Heterocycle Synthesis Using an Internal Oxidant: Improved Reactivity and Mechanistic Studies. *J. Am. Chem. Soc.* **2011**, *133* (16), 6449–6457. https://doi.org/10.1021/ja201143v.

(89) Churchill, D. G.; Janak, K. E.; Wittenberg, J. S.; Parkin, G. Normal and Inverse Primary Kinetic Deuterium Isotope Effects for C–H Bond Reductive Elimination and Oxidative Addition Reactions of Molybdenocene and Tungstenocene Complexes: Evidence for Benzene σ-Complex Intermediates. *J. Am. Chem. Soc.* **2003**, *125* (5), 1403–1420. https://doi.org/10.1021/ja027670k.

(90) Anderson, S. N.; Cooksey, C. J.; Holton, S. G.; Johnson, M. D. Substitution and Cleavage in the Reaction of Some Benzyl(Carbonyl)Metal Complexes with Trifluoroacetic Acid. *J. Am. Chem. Soc.* **1980**, *102* (7), 2312–2318. https://doi.org/10.1021/ja00527a031.

(91) Wu, F.; Deraedt, C.; Cornaton, Y.; Contreras-Garcia, J.; Boucher, M.; Karmazin, L.; Bailly, C.; Djukic, J.-P. Making Base-Assisted C–H Bond Activation by Cp*Co(III) Effective: A Noncovalent Interaction-Inclusive Theoretical Insight and Experimental Validation. *Organometallics* **2020**, *39* (14), 2609–2629. https://doi.org/10.1021/acs.organomet.0c00253.

(92) Rosini, G. P.; Soubra, S.; Vixamar, M.; Wang, S.; Goldman, A. S. Kinetics of Photochemical Alkane Dehydrogenation Catalyzed by Rh(PMe3)2(CO)Cl: Implications Concerning the C–H Bond Activation Step. *J. Organomet. Chem.* **1998**, *554* (1), 41–47.

(93) McKay, A. I.; Bukvic, A. J.; Tegner, B. E.; Burnage, A. L.; Martínez-Martínez, A. J.; Rees, N. H.; Macgregor, S. A.; Weller, A. S. Room Temperature Acceptorless Alkane Dehydrogenation from Molecular σ-Alkane Complexes. *J. Am. Chem. Soc.* **2019**, *141* (29), 11700–11712. https://doi.org/10.1021/jacs.9b05577.

(94) Sur, A.; Jernigan, N. B.; Powers, D. C. Kinetic Probes of the Origin of Activity in MOF-Based C–H Oxidation Catalysis. *ACS Catal.* **2022**, 3858–3867. https://doi.org/10.1021/acscatal.1c05415.

(95) Fulmer, G. R.; Miller, A. J. M.; Sherden, N. H.; Gottlieb, H. E.; Nudelman, A.; Stoltz, B. M.; Bercaw, J. E.; Goldberg, K. I. NMR Chemical Shifts of Trace Impurities: Common Laboratory Solvents, Organics, and Gases in Deuterated Solvents Relevant to the Organometallic Chemist. *Organometallics* **2010**, *29* (9), 2176–2179. https://doi.org/10.1021/om100106e.

(96) Kohen, A.; Klinman, J. P. Enzyme Catalysis: Beyond Classical Paradigms. *Acc. Chem. Res.* **1998**, *31* (7), 397–404. https://doi.org/10.1021/ar9701225.

(97) Kohen, A.; Roston, D.; Stojković, V.; Wang, Z. Kinetic Isotope Effects in Enzymes. In *Encyclopedia of Analytical Chemistry*; American Cancer Society, 2010. https://doi.org/10.1002/9780470027318.a9161.

(98) Towns, J.; Cockerill, T.; Dahan, M.; Foster, I.; Gaither, K.; Grimshaw, A.; Hazlewood, V.; Lathrop, S.; Lifka, D.; Peterson, G. D.; Roskies, R.; Scott, J. R.; Wilkins-Diehr, N. XSEDE: Accelerating Scientific Discovery. *Computing in Science & Engineering* **2014**, *16* (05), 62–74. https://doi.org/10.1109/MCSE.2014.80.

(99) Frisch, M. J.; Trucks, G. W.; Schlegel, H. B.; Scuseria, G. E.; Robb, M. A.; Cheeseman, J. R.; Scalmani, G.; Barone, V.; Petersson, G. A.; Nakatsuji, H. Gaussian 16 Revision B. 01. 2016; Gaussian Inc. *Wallingford CT* **46**.

(100) Dennington, Roy; Keith, Todd A.; Millam, John M. GaussView, Version 6.

(101) Becke, A. D. A New Mixing of Hartree–Fock and Local Density-functional Theories. *J. Chem. Phys.* **1993**, *98* (2), 1372–1377. https://doi.org/10.1063/1.464304.

(102) Miehlich, B.; Savin, A.; Stoll, H.; Preuss, H. Results Obtained with the Correlation Energy Density Functionals of Becke and Lee, Yang and Parr. *Chem. Phys. Lett.* **1989**, *157* (3), 200–206. https://doi.org/10.1016/0009-2614(89)87234-3.

(103) Lee, C.; Yang, W.; Parr, R. G. Development of the Colle-Salvetti Correlation-Energy Formula into a Functional of the Electron Density. *Phys. Rev. B* **1988**, *37* (2), 785–789. https://doi.org/10.1103/PhysRevB.37.785.

(104) Schäfer, A.; Horn, H.; Ahlrichs, R. Fully Optimized Contracted Gaussian Basis Sets for Atoms Li to Kr. *J. Chem. Phys.* **1992**, *97* (4), 2571–2577. https://doi.org/10.1063/1.463096.

(105) Schäfer, A.; Huber, C.; Ahlrichs, R. Fully Optimized Contracted Gaussian Basis Sets of Triple Zeta Valence Quality for Atoms Li to Kr. *J. Chem. Phys.* **1994**, *100* (8), 5829–5835. https://doi.org/10.1063/1.467146.

(106) Weigend, F.; Ahlrichs, R. Balanced Basis Sets of Split Valence, Triple Zeta Valence and Quadruple Zeta Valence Quality for H to Rn: Design and Assessment of Accuracy. *Phys. Chem. Chem. Phys.* **2005**, *7* (18), 3297–3305. https://doi.org/10.1039/B508541A.

(107) Weigend, F. Accurate Coulomb-Fitting Basis Sets for H to Rn. *Phys. Chem. Chem. Phys.* **2006**, *8* (9), 1057–1065. https://doi.org/10.1039/B515623H.

variable large KIE

reaction is not bimolecular or elementary